Original Article

Sodium Butyrate Inhibits Necroptosis by Regulating MLKL via E2F1 in Intestinal Epithelial Cells of Liver Cirrhosis

Yimeng Zhou[1,2], Yang Ding[1,2], Yanwei Li[1], Qiuju Sheng[1], Chao Han[1], Yaoxin Fan[1,2], Ziyi Wang[1], Bingchao Lu[1], Xiaoguang Dou[1,2]* and Chong Zhang[1,2]*

[1]Department of Infectious Diseases, Shengjing Hospital of China Medical University, Shenyang, Liaoning, China; [2]Key Laboratory of Viral Hepatitis, Shengjing Hospital of China Medical University, Shenyang, Liaoning, China

Abstract

Background and Aims: Necroptosis is critical for regulating intestinal epithelial cells (IECs). Butyric acid (BA), produced during intestinal microbial metabolism, protects the intestinal epithelial barrier. However, whether necroptosis occurs in IECs during liver cirrhosis and whether sodium butyrate (NaB) can regulate necroptosis have not yet been reported. In this study, we aimed to investigate whether IECs undergo necroptosis in cirrhosis and whether NaB can regulate necroptosis and the related regulatory mechanisms. ***Methods:*** Serum levels of RIPK3, MLKL, and Zonulin, as well as fecal BA levels, were measured and correlated in 48 patients with liver cirrhosis and 20 healthy controls. A rat model of liver cirrhosis was established, and NaB was administered. The expressions of MLKL, p-MLKL, and tight junction proteins were measured. We conducted an *in vitro* investigation of the effect of NaB on necroptosis in the HT29 cell line. ***Results:*** Serum levels of RIPK3, MLKL, and Zonulin in the liver cirrhosis group were higher, while fecal BA levels were lower than those in the control group. Zonulin levels were positively correlated with RIPK3 and MLKL levels, while fecal BA levels were negatively correlated with serum MLKL levels, but not with RIPK3 levels. NaB reduced the mRNA and protein expression of MLKL but had no effect on RIPK1 and RIPK3 in vitro. Rescue experiments demonstrated that NaB inhibited necroptosis through E2F1-mediated regulation of MLKL. ***Conclusions:*** NaB alleviates intestinal mucosal injury and reduces necroptosis in IECs in liver cirrhosis. It also inhibits the necroptosis of IECs and protects the intestinal barrier by reducing E2F1 expression and downregulating MLKL expression levels. These results can be employed to develop a novel strategy for treating complications arising from liver cirrhosis.

Citation of this article: Zhou Y, Ding Y, Li Y, Sheng Q, Han C, Fan Y, *et al*. Sodium Butyrate Inhibits Necroptosis by Regulating MLKL via E2F1 in Intestinal Epithelial Cells of

Liver Cirrhosis. J Clin Transl Hepatol 2024. doi: 10.14218/JCTH.2024.00221.

Introduction

Liver cirrhosis is the 11th most common cause of death globally, with approximately two million deaths annually, accounting for 3.5% of the global mortality rate.[1] Portal hypertension in cirrhosis adversely affects blood circulation in the intestinal mucosa, causing dysbiosis of the intestinal microbiota and disrupting intestinal barrier function. As a result, various complications arise, such as hepatic encephalopathy, spontaneous bacterial peritonitis, and hepatorenal syndrome. Therefore,[2] the role and function of the intestinal mucosal barrier in the development and maintenance of cirrhosis are attracting increasing attention from researchers.

The intestinal mucosal barrier is mainly composed of mucus, intestinal epithelial cells (IECs), and intercellular tight junctions. In many diseases, including cirrhosis, disruption of intercellular tight junction proteins (including Occludin, Claudin, and ZO-1) increases intestinal permeability, allowing microbes to translocate from the intestinal lumen and causing subsequent inflammation and immune system activation.[3,4] IECs maintain the homeostasis of the intestinal epithelium by regulating cell death. Various programmed cell death mechanisms, including apoptosis, necroptosis, pyroptosis, ferroptosis, and autophagy, play important roles in regulating the intestinal epithelium.[5–9] Necroptosis is a newly discovered form of regulated cell death, with RIPK3 and MLKL as the key molecules responsible for its execution. The translocation of phosphorylated MLKL to the inner side of the cell membrane, disrupting cell membrane integrity, is a critical step in necroptosis.[10] Increasing evidence suggests that necroptosis plays an important role in regulating the intestinal epithelial barrier and is associated with IEC injury in various diseases, including cirrhosis. Currently, the most extensive research is being conducted in the field of inflammatory bowel disease.[11] Other conditions, such as mesenteric ischemia-reperfusion, sepsis, colorectal tumors, and lethal ileitis, are also associated with IEC necroptosis.[12–15] However, whether necroptosis is associated with the intestinal mucosa in cirrhosis and whether necroptosis occurs in IECs during cirrhosis have not yet been reported.

Cirrhosis is closely related to the gut–liver axis, exhibiting

a unique bidirectional relationship. It has been shown that gut dysbiosis and subclinical intestinal damage are common in cirrhosis. Disorders of the gut microbiota and intestinal barrier damage lead to bacterial translocation, causing local inflammation in the intestinal wall and liver and triggering systemic inflammation. Consequently, this results in increased circulating blood volume and portal pressure, which aggravates portal hypertension.[16] The intestinal microbiota and its metabolites are considered to contribute to some complications of cirrhosis.[17] Short-chain fatty acids (SCFAs), such as acetic acid, propionic acid, and butyric acid (BA), are metabolites produced by the intestinal microbiota. SCFAs may play a pathogenic role in inflammation and liver diseases.[18] Many symbiotic strains also produce SCFAs while metabolizing insoluble fibers. Butyrate is a nutrient for IECs; it promotes cell regeneration, enhances the expression of tight junctions, and reduces macrophage inflammatory responses, thereby protecting intestinal barrier function.[19] Sodium butyrate (NaB) regulates cell death, including apoptosis, ferroptosis, and pyroptosis.[20–22] However, the effect of NaB on necroptosis has not yet been reported.

Cirrhosis is closely related to intestinal barrier injury, while butyrate has a protective effect on the intestinal barrier. However, it is still not known whether butyrate can protect the intestinal barrier by reducing necroptosis. In an attempt to develop new strategies for treating cirrhosis and its complications, this study investigates whether IECs undergo necroptosis in cirrhosis and whether NaB can regulate necroptosis and the related regulatory mechanisms.

Methods

Patients

We enrolled 48 patients with liver cirrhosis from the Department of Infectious Diseases at Shengjing Hospital of China Medical University, admitted from August 2019 to December 2020. Additionally, we recruited 20 healthy controls from the Health Examination Center of the same hospital. Patients with concurrent inflammatory bowel disease, intestinal tumors, or any other conditions leading to intestinal mucosal injury were excluded. Those with conditions that could significantly affect SCAFs, such as gastrointestinal bleeding and portal vein thrombosis, were also excluded. Discarded blood and fecal specimens from routine tests conducted upon patient admission were utilized. Blood samples were collected in the morning under fasting conditions. We gathered clinical data, including demographic information (gender, age, and date of admission), medical history (relevant risk factors for intestinal barrier injury, such as gastrointestinal diseases), and information on liver function, coagulation profile, and imaging data obtained after admission. Liver function was tested using the Beckman Coulter 5400 automatic biochemical immunoassay analyzer, while the coagulation profile was obtained using the ACL-TOP-700 automatic blood coagulation analyzer (Werfen, Spain).

Serum-level detection of MLKL, RIPK3, and Zonulin by ELISA

Peripheral venous blood samples were collected from each study participant in the early morning while fasting. The samples were centrifuged at 3,500 rpm for approximately 10 m, and the supernatant was collected. ELISA assays were performed by strictly adhering to the manufacturers' instructions.[23] The test kits used were the MLKL ELISA kit (JL14772, Jianglai Biotech, China), the RIPK3 ELISA kit (Shanghai Enzyme-linked Biotechnology Co., Ltd.), and the Zonulin ELISA

kit (JL14924, Jianglai Biotech, China).

BA detection in fecal samples

Fecal samples were collected from the study participants in the morning, rapidly frozen in liquid nitrogen for 15 m, and stored at −80°C. BA (B103500, Merck, Germany) was precisely weighed and dissolved in ether to prepare a series of standard solutions of varying concentrations. A reference substance, 2-methylvaleric acid (M117868, Aladdin, China), was precisely weighed and dissolved in ether to prepare an internal standard solution. A specific amount of the sample was weighed and homogenized with deionized water, followed by vortex mixing and centrifugation. The supernatant was then transferred and mixed with 50% sulfuric acid, ether, and the internal standard solution. After vortexing and centrifugation, the supernatant was collected for GC-MS analysis using an Agilent 7890B-5977B GC-MS system.[24] Quantitative testing of the known characteristic ions was performed using the selected ion monitoring mode. The content was calculated using standard curve integration with MassHunter software.

Animal experiments

Male Sprague-Dawley (SD) rats, aged five to six weeks and weighing 160–180 g, were purchased from Beijing HuaFu-Kang Biotechnology Co., Ltd. The rats were housed in a specific pathogen-free animal facility at Shengjing Hospital of China Medical University, maintained at 23 ± 2°C, 60% ± 5% humidity, and on a 12-h light–dark cycle. They were fed standard rat chow, and 1.5 mmol/L phenobarbital was added to their drinking water. The rats' body weights increased to over 200 g after 10–14 days. They were then administered CCl_4 by gavage once a week. After approximately eight weeks, the rats were euthanized, and their liver tissues were collected.[25] Hematoxylin and eosin (HE) staining was performed on the liver tissues, and typical pseudo-lobule formation was observed under a microscope, confirming the successful establishment of the liver cirrhosis model. Fifteen rats were randomly divided into three groups: untreated control group (blank control group), liver cirrhosis group (negative control group), and liver cirrhosis + NaB group (experimental group), with five rats in each group. In the experimental group, after 8 weeks of liver cirrhosis, 200 mg/kg·d of NaB was added to the drinking water, while the other groups were fed a normal diet for an additional three weeks. All rats were euthanized by cervical dislocation under deep anesthesia after 11 weeks of feeding. The BA levels in the feces of the rats in each group before euthanasia were measured using GC-MS.

HE Staining

The liver and colon tissues of the rats were fixed in 4% paraformaldehyde for 48 h. After dehydration in varying concentrations of ethanol and xylene, the tissues were embedded in paraffin, sectioned, and flattened. After overnight incubation, the sections were deparaffinized in different concentrations of xylene and ethanol. HE staining was performed using an HE staining kit (G1120, Solarbio, China), followed by immersion in varying concentrations of ethanol and xylene. Neutral gum was used for mounting.[26] The specimens were observed using a bright-field microscope with an image capture system (ECLIPSE Ni, Nikon Corporation, Japan).

Evaluation of colon tissue pathological injury

The modified Chiu's scoring system[27] was used to evaluate the intestinal pathological injury of the colon tissue stained

with HE (Supplementary Table 1).

Western blot

Western blot analysis was performed according to previously established methods.[28] The reagents used in this experiment are listed in the Supplementary File 1. RIPA protein lysis buffer, PMSF, and phosphatase inhibitor were employed to extract cellular or tissue proteins. Protein concentration was measured using a BCA protein assay kit. The membrane was analyzed using a chemiluminescence imaging system (5200Multi, Shanghai Tanon Technology, China). Band intensity was quantified using Image J 1.46r software.

Immunohistochemistry

Paraffinized sections of colon tissue from each group were sequentially deparaffinized in varying concentrations of xylene and ethanol, followed by microwave heating in a citrate antigen retrieval solution. The sections were processed using a universal two-step immunohistochemical staining kit (PV-9000, ZSGB-BIO, China) and a DAB working solution (ZLI-9018, ZSGB-BIO, China) for visualization.[29] Images were captured and saved using NIS-Elements AR Analysis 4.50.00 software. The image-pro plus 6.0 software was used to analyze the images and calculate the average optical density (mean intensity: IOD value/area) of each image.

Cell culture

The colon cancer cell line (HT29) was obtained from the Shanghai Cell Bank, Chinese Academy of Sciences. The culture medium consisted of 90% McCoy's 5A Medium (01-075-1ACS, BI, Israel), 10% FBS (10099-141C, Gibco, USA), and 1% penicillin–streptomycin solution (100×) (P1400, Solarbio, China). The cells were cultured in a humidified atmosphere at 37°C with 5% CO_2 in a cell culture incubator.

CCK8 assay

The CCK8 assay kit (K1018, APEXBIO, USA) was used to assess the cytotoxicity of different concentrations (0, 1, 2, 4, 8, 16, and 32 mmol/L) of NaB. Absorbance at 450 nm was measured using a microplate reader (S1LFA, BioTek, USA). Data analysis was performed using the formula: Cell viability (%) = $[(As - Ab)/(Ac - Ab)]*100$, where *As* is the absorbance of the experimental well (containing cells, the culture medium, CCK-8, and the test compound), *Ab* is the absorbance of the blank well (containing the culture medium and CCK-8), and *Ac* is the absorbance of the control well (containing cells, the culture medium, and CCK-8).[30]

Construction of a necroptosis model

Please refer to the Supplementary File 2.

qRT-PCR

TSZ (1:1,000) was cultured for 4 h to induce necroptosis in the HT29 cell line, and 4 mM NaB was added for the subsequent 12 h. RNA was extracted using the TRIzol method, followed by reverse transcription using a PCR machine (6331, Eppendorf, Germany) and the GoScript™ Reverse Transcription System (A5001, Promega, USA). qRT-PCR was performed using PCR primers (Sangon Biotech, China) listed in Supplementary Table 2 and the PCR GoTaq® qRT-PCR Master Mix (A6001, Promega, USA). The experiment was conducted using the Roche Cobas Z480 fluorescent quantitative PCR instrument. The relative difference in gene expression was calculated using the $2^{-\Delta\Delta Ct}$ method.[31]

Prediction of transcription factors interacting with target proteins

The GSE45220 dataset (HT-29 cells stimulated with NaB and unstimulated control, n = 3 in each group for 24 h; RNA extracted from these cells was hybridized on Affymetrix microarrays) and the GSE61429 dataset (butyrate-treated vs. untreated HT-29 cells; biological replicates: two control replicates and two 24-h butyrate-treated replicates) from the GEO database (https://www.ncbi.nlm.nih.gov/geo/) were selected to identify common differentially expressed genes.[32,33] Differential gene expression analysis was performed using the "limma" R package in R software (version 4.3.2).[34] The JASPAR database (https://jaspar.genereg.net/)[35] (with a UCSC score above 400) and the GRNdb database (http://www.grndb.com/)[36] were used to predict the transcription factors interacting with MLKL. The transcription factors predicted by both databases and the common differentially expressed genes from the datasets were considered the predicted transcription factors.

Plasmid transfection

Logarithmic-growth-phase HT29 cells were seeded at 4×10^5 cells per well in a 6-well plate and incubated in McCoy's 5A Medium without antibiotics. Transfection was performed after 24 h using the E2F1-overexpression plasmid (HG17394-NF, Sino Biological, China) and an empty vector. The transfection was conducted according to the instructions of the Attractene Transfection Reagent (301005, Qiagen, Germany).[37] Both the transfection reagent and DNA were dissolved in the Opti-MEM medium (31985-062, Gibco, USA).

RNAi

Fluorescently labeled siRNA (synthesized by Sangon Biotech, China; the sequence is listed in Supplementary Table 3) was used as the experimental group, while cells transfected with a scrambled sequence of siRNA-NC served as the negative control group. The transfection procedure was conducted using the RNA transfection reagent (R19425015, Golden Transfer Technology, China).[38]

Dual-luciferase reporter assay

The promoter region of MLKL was cloned into the pGL3-Basic vector, and an E2F1 gene expression vector was constructed (Wanleibio, China). The following groups were established: A. pGL3-Basic + empty vector + pRL-TK vector transfection group; B. pGL3-Basic + E2F1 + pRL-TK vector transfection group; C. pGL3-Basic-MLKL promoter + empty vector + pRL-TK vector transfection group; D. pGL3-Basic-MLKL promoter + E2F1 + pRL-TK vector transfection group. After 48 h of cell transfection, the dual-luciferase assay was performed using a dual-luciferase reporter assay kit (KGAF040, KeyGEN BioTECH, China) to measure dual-luciferase activity.[39]

Chromatin immunoprecipitation (ChIP) assays

Experimental reagents included the ChIP Assay Kit (P2078, Beyotime, China). The experimental grouping was as follows: Group A: Experimental group with the addition of E2F1 antibody, using specific primers for RT-PCR. Group B: RT-Input1, using specific primers for RT-PCR to test binding efficiency. Group C: Negative control group with the addition of host IgG for E2F1 antibody, using specific primers for RT-PCR. Group D: PCR negative control group, using ddH_2O as a template with specific primers for RT-PCR. Group E: Positive control group with the addition of RNA polymerase II antibody, using GAPDH primers (primer sequences: F: TAC-

Table 1. Clinical baseline characteristics of study participants

Parameters	Cirrhosis group	Healthy control group	*p*-value
Age (years)	56.94 ± 10.42	60.25 ± 6.76	0.25
Gender			1
Male	28/48 (58.33%)	11/20(55.00%)	
Female	20/48 (41.67%)	9/20(45.00%)	
Etiology of Cirrhosis			
HBV	36 (75.00%)	–	N
HCV	4 (8.33%)	–	N
PBC	3 (6.25%)	–	N
Others	5 (10.42%)	–	N
Child-Pugh Class			
A	14 (29.17%)	–	N
B	19 (39.58%)	–	N
C	15 (31.25%)	–	N

HBV, hepatitis B virus; HCV, hepatitis C virus; PBC, primary biliary cholangitis.

TAGCGGTTTTACGGGCG, R: TCGAACAGGAGGAGCAGAGAGC-GA) for RT-PCR. Group F: RT-Input2, using GAPDH primers for RT-PCR to test the PCR system. Sonication of samples, chromatin immunoprecipitation, and PCR amplification of the target gene sequence (F: CTGGAGAATCGCTTGAACCC, R: TT-TATTTTGTCCCTGCCTGA) were performed. Experimental procedures were strictly followed according to the manual.[40]

Molecular docking

The molecular structure of BA was retrieved from the PubChem database (https://pubchem.ncbi.nlm.nih.gov/). Chem3D was used for format conversion and energy minimization. All structures were imported into the Schrödinger software. The structures underwent hydrogenation, structural optimization, and energy minimization and were saved as the ligand molecule database. The protein structure of E2F1 (PDB ID: 2AZE) was retrieved from the RCSB database (https://www.rcsb.org/). Protein structure processing was performed on the Maestro 11.9 platform, using Schrödinger's Protein Preparation Wizard to remove crystal water, add missing hydrogen atoms, repair missing bond information, repair missing peptide segments, and perform energy minimization and geometric structure optimization.[41,42] Molecular docking was conducted using the Glide module in the Schrödinger Maestro software. Protein processing was performed using the Protein Preparation Wizard module to preprocess, optimize, and minimize the receptor (using the OPLS3e force field for restrained minimization). All molecules were prepared according to the default settings of the LigPrep module. The predicted binding site of the protein was selected as the center of gravity of a 12 Å box. Molecular docking and screening were performed using the standard precision docking method.[43] The interaction mode between BA and E2F1 was analyzed to determine the compound–protein residue interactions. Additionally, the docking scores of the compounds were considered to infer whether the screened compounds exhibited any activity.

Statistical analysis

Statistical analysis of the data was conducted using Graph-Pad Prism 8.0.1. When the data from two groups followed a normal distribution, the *t*-test was used to compare dif-ferences; otherwise, the Mann–Whitney test was employed. For data from more than two groups that followed a normal distribution, ANOVA analysis was chosen; otherwise, the Kruskal–Wallis test was applied. When the data from the two groups did not follow a normal distribution, Spearman correlation analysis was conducted. A *p*-value of <0.05 was considered statistically significant.

Results

NaB alleviates the necroptosis in the intestinal mucosa of patients with liver cirrhosis

The clinical baseline characteristics of the study participants (48 patients with liver cirrhosis and 20 healthy controls) are listed in Table 1. The serum levels of RIPK3, MLKL, and Zonulin in both groups were measured using ELISA (Fig. 1A–C). The cirrhosis group had significantly higher levels of RIPK3 [(391.15 ± 73.87) pg/mL], MLKL {[1.49, (0.79–3.19)] ng/mL}, and Zonulin {[271.59, (157.76–401.38)] ng/mL} compared to the healthy control group {(313.19 ± 59.60) pg/mL, [0.46, (0.27–0.57)] ng/mL, and [23.79, (19.73–33.60)] ng/mL, respectively ($p < 0.0001$)}. Zonulin was used as a biological marker for evaluating intestinal mucosal injury. Spearman correlation analysis (Fig. 1E, F) showed a positive correlation between Zonulin and MLKL, as well as with RIPK3 levels ($R = 0.34$, $R = 0.40$) ($p < 0.05$).

The levels of BA in the feces of both groups were measured using GC-MS. The results showed that the BA level in the cirrhosis group [1.02, (0.39–1.54)] μg/mL was lower than that in the healthy control group {[1.35, (1.02–2.13)] μg/mL} ($p < 0.05$) (Fig. 1D). The Spearman correlation analysis indicated a negative correlation between fecal BA levels and serum MLKL levels ($R = −0.27$) ($p < 0.05$) (Fig. 1H). However, the correlation analysis with RIPK3 levels showed no statistical significance ($p > 0.05$) (Fig. 1G).

Necroptosis in the IECs of cirrhotic rats can be alleviated by NaB

The cirrhotic rat model was established, and typical pseudolobule formation was observed in the rat liver under a microscope (Fig. 2A, D). The BA levels in the feces of each group
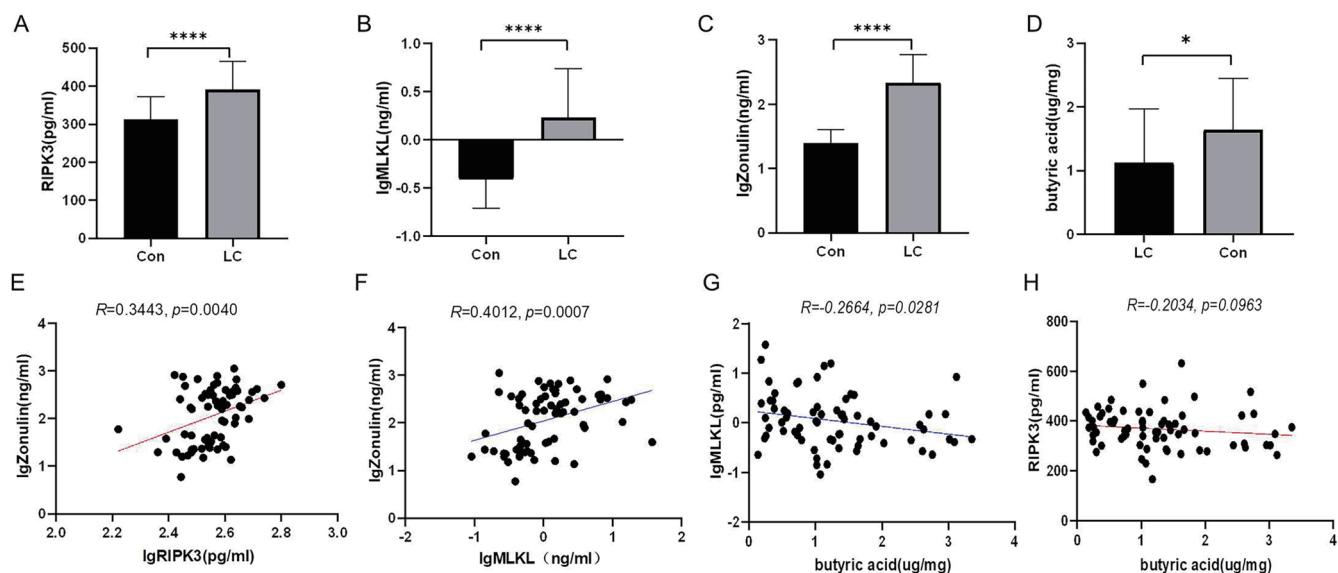
Fig. 1. Correlation of BA and necroptosis in the intestinal mucosa of patients with liver cirrhosis. (A–C) Serum levels of RIPK3, MLKL, and Zonulin were measured by ELISA in the cirrhosis group (n = 48) and healthy control group (n = 20). (D) BA levels in the feces were measured using GC-M. (E, F) Spearman correlation analysis between Zonulin and MLKL, as well as with RIPK3 levels. (G, H) Spearman correlation analysis between fecal BA levels and serum MLKL levels, as well as with RIPK3 levels. BA, butyric acid; ELISA, enzyme-linked immunosorbent assay; GC-MS, gas chromatography-mass spectrometry; *p < 0.05, ****p < 0.0001.

of rats were measured using GC-MS. The cirrhosis group had lower levels of BA (0.27 ± 0.04) compared to the cirrhosis + NaB group (0.42 ± 0.16) and the blank control group (0.54 ± 0.20) (p < 0.05) (Fig. 2E).

HE staining of the colon tissues and scoring of intestinal mucosal injury showed that the cirrhosis group had the most severe mucosal injury (p < 0.05). The intestinal mucosal injury was reduced in the group receiving NaB (2.6 ± 0.55) compared to the cirrhosis group (3.80 ± 0.84) (p < 0.05) (Fig. 2F).

The expression of tight junction proteins was detected by Western blot analysis. In the cirrhosis group, the expressions of Claudin-1 and Occludin were lower than in the blank control group (p < 0.05), while the expression of ZO-1 showed no statistical difference (p > 0.05). Unlike the cirrhosis group, the addition of NaB increased the expression of Claudin-1 (p < 0.05), with no statistical difference in the expressions of ZO-1 and Occludin (p > 0.05) (Fig. 2G–L).

Western blot and immunohistochemical analyses showed that the cirrhosis group had higher expressions of MLKL and p-MLKL than the blank control group (p < 0.05). In contrast, the addition of NaB to the cirrhosis group decreased the expression of MLKL (p < 0.05) (Fig. 2M–R).

A necroptosis model was established

Annexin V$^+$/PI$^+$ cells were defined as late apoptotic and necroptotic cells, whereas Annexin V$^+$/PI$^-$ cells were categorized as early apoptotic cells.[44] When cells were treated with the TSZ method at 0 h, 4 h, 8 h, and 12 h, the proportions of (Annexin V$^+$/PI$^-$, Annexin V$^+$/PI$^+$) for flow cytometry were (1.30 ± 0.38, 7.72 ± 3.31), (10.35 ± 3.65, 15.48 ± 2.92), (12.83 ± 1.00, 15.78 ± 1.68), and (16.50 ± 2.01, 18.05 ± 4.19), respectively. The results indicate that the TSZ method can induce necroptosis in the HT29 cell line at 4 h (p < 0.05). There were no statistically significant differences at 8 h and 12 h compared to 4 h (p > 0.05) (Supplementary Fig. 1C). Western blot analysis showed higher expressions of p-MLKL at 4 h than at 0 h, indicating consistent results (Supplemen-

tary Fig. 1D-F). CCK8 results showed that the EC$_{50}$ of NaB at 24 h and 48 h were 3.2 and 6.0 mM, respectively. No significant changes in HT29 cell survival were observed with up to 8.0 mM of NaB at 12 h (Supplementary Fig. 1A, B). Cells were treated with NaB at concentrations of 0, 1.0, 2.0, 4.0, and 8.0 mmol/L and induced to undergo necroptosis using the TSZ method. The proportions of (Annexin V$^+$/PI$^-$, Annexin V$^+$/PI$^+$) were (17.37 ± 5.80, 12.28 ± 3.22), (16.50 ± 6.35, 10.38 ± 0.93), (28.50 ± 12.10, 9.45 ± 1.54), (35.37 ± 12.09, 8.4 ± 0.38), and (26.77 ± 12.24, 7.63 ± 0.95), respectively. Flow cytometry (Annexin V/PI) showed that 4 and 8 mM of NaB reduced necroptosis (p < 0.05), while the Western blot analysis indicated a significant effect at 4 mM (Supplementary Fig. 1G-J). Therefore, 4 mM of NaB was selected as the effective concentration.

NaB reduces the mRNA and protein expression levels of MLKL

The mRNA and protein expressions of the RIPK1/RIPK3/MLKL pathway were measured by qRT-PCR and Western blot. Compared to the necroptosis group, the addition of NaB decreased the mRNA and protein expression of MLKL (p < 0.05), while the expressions of RIPK1/p-RIPK1 and RIPK3/p-RIPK3 showed no statistical difference (p > 0.05) (Fig. 3).

E2F1 regulates the expression of MLKL

The differential gene analysis of the GSE45220 and GSE61429 datasets in the GEO database identified 375 differentially expressed genes with an adjusted p-value below 0.05 and |log2(fold change)| above 0.5 (Fig. 4A, Supplementary Table 4). Using the JASPAR database (with a UCSC score of >400) and the GRNdb database, 17 transcription factors were identified that can bind to MLKL. E2F1 and SPDEF were selected as the common transcription factors for the intersection of the differentially expressed genes (Fig. 4B). E2F1 is associated with the regulation of the cell cycle. We next investigated whether it plays a role in the regulation of MLKL-mediated necroptosis.
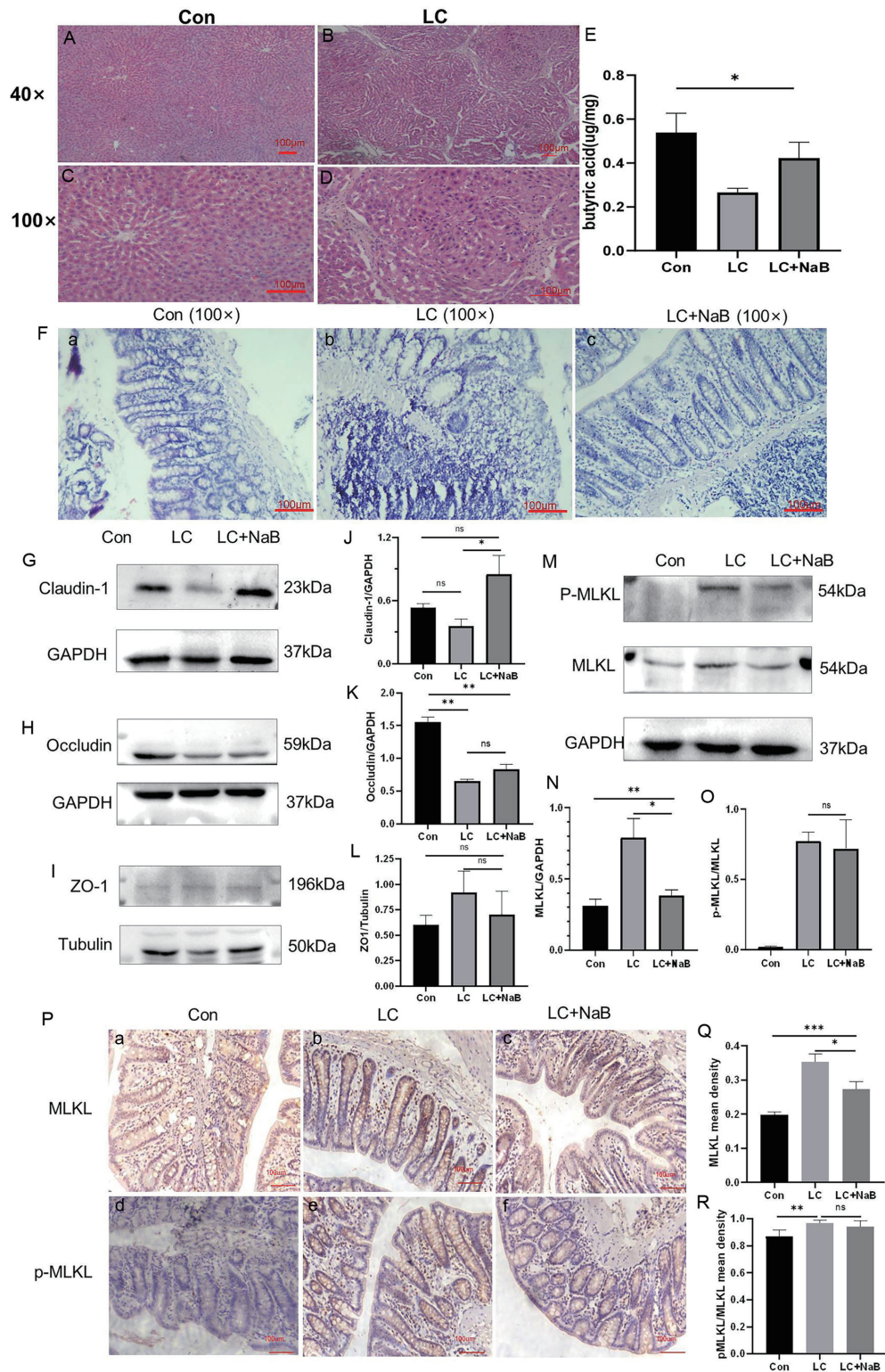
Fig. 2. The effects of NaB on necroptosis in the IECs of cirrhotic rats. Fifteen male SD rats were randomly divided into three groups, with five rats in each group: Con, blank control group; LC, cirrhosis group (negative control group); LC + NaB, cirrhosis plus sodium butyrate group (experimental group). (A–D) HE staining of liver tissue. (E) GC-MS was used to measure the BA levels in the feces of rats from each group 24 h before euthanasia. (F) HE staining of intestinal mucosa. (G–L) Western blot analysis was used to examine the expressions of Claudin-1, Occludin, and ZO-1. (M–R) Western blot and immunohistochemical analysis were used to examine the expression of MLKL and p-MLKL. NaB, sodium butyrate; IECs, intestinal epithelial cells; HE, Hematoxylin and eosin; GC-MS, gas chromatography-mass spectrometry; BA, bile acid; $*p < 0.05$, $**p < 0.01$, $***p < 0.001$, ns, no significance.
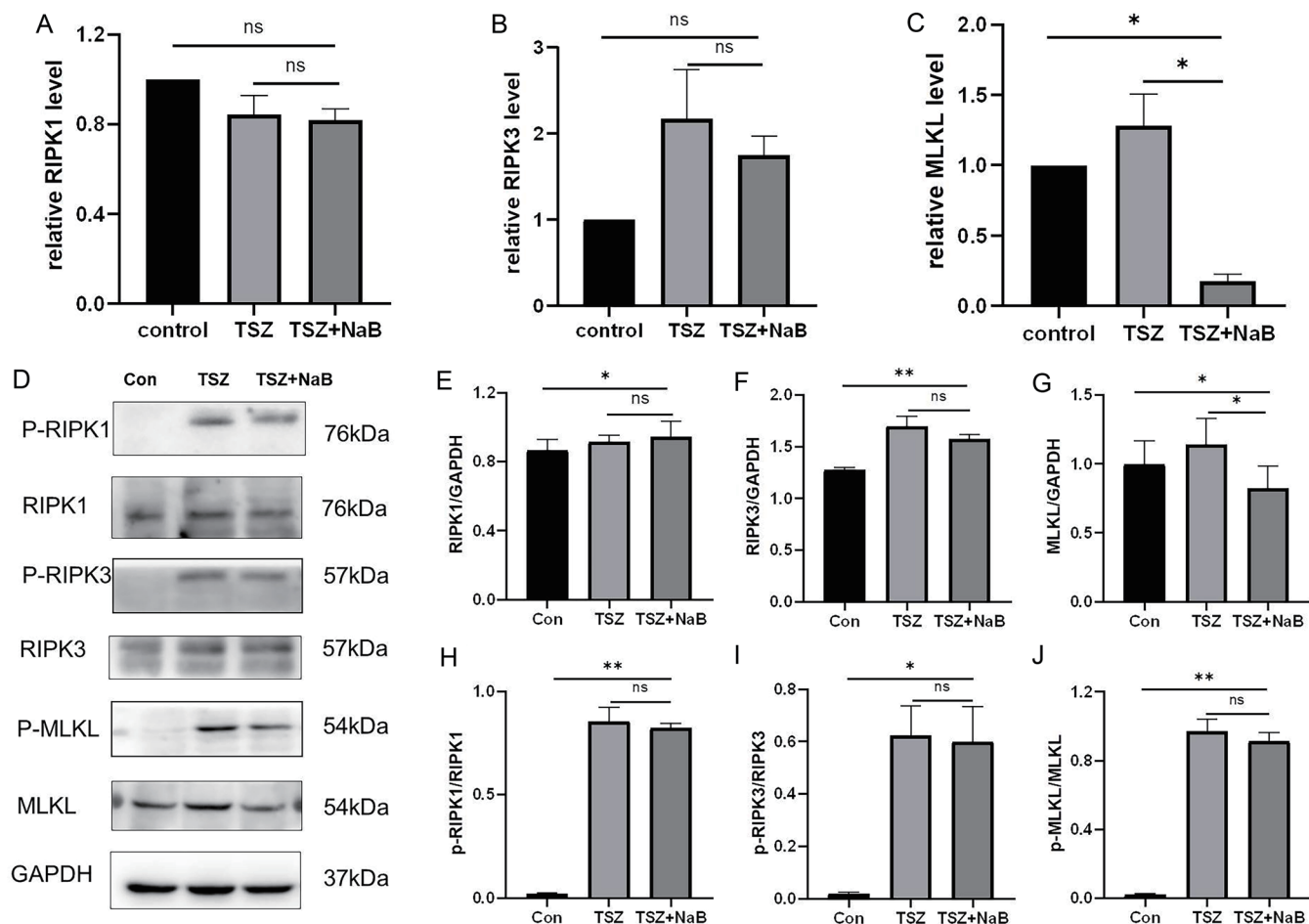
Fig. 3. The effects of NaB on the RIPK1/RIPK3/MLKL pathway. (A–C) mRNA expressions of RIPK1, RIPK3, and MLKL were measured by qRT-PCR. (D–J) Protein expressions of the RIPK1/RIPK3/MLKL pathway were measured by Western blot. NaB, sodium butyrate; Con, control group; TSZ, necroptosis group; TSZ + NaB, NaB + necroptosis group; *$p < 0.05$, **$p < 0.01$, ns, no significance.

E2F1-overexpression plasmids and empty plasmids were transfected into HT29 cell lines. The mRNA and protein expressions of MLKL were measured by qRT-PCR and Western blot, respectively. Overexpression of E2F1 significantly increased the mRNA and protein expressions of MLKL ($p < 0.05$) (Fig. 4C–G), indicating that E2F1 upregulates the mRNA and protein expressions of MLKL.

Three different siRNA-E2F1 and siRNA-NC (negative control) were transfected into HT29 cell lines. The mRNA and protein expression levels ($p < 0.05$) of E2F1 decreased in the siRNA-E2F1-2 and siRNA-E2F1-3 groups. Additionally, the mRNA and protein expressions ($p < 0.05$) of MLKL also decreased in these two groups, indicating that the knockdown of E2F1 downregulates the expression of MLKL (Fig. 4H–L).

The promoter region of MLKL was cloned into the pGL3-Basic vector, and an E2F1 gene expression vector was constructed. HT29 cells were transfected during their logarithmic growth phase. After 48 h, the activity of the dual-luciferase reporter was measured using a dual-luciferase reporter assay kit. The results showed that the transcription factor E2F1 binds to the promoter region of the target gene MLKL (****$p < 0.0001$) (Fig. 4M).

We predicted the binding sites of E2F1 on MLKL using the JASPAR website. Based on the prediction results, we selected a high-scoring binding site (Sequence ID: NC_000016.

10:c74702862-74700862, 313-324) to design primers. The ChIP experiment results (Fig. 4N) confirmed that E2F1 can bind to the promoter region of MLKL.

NaB alleviates necroptosis by downregulating MLKL via E2F1

The mRNA and protein expressions of E2F1 decreased in the NaB group ($p < 0.05$) (Fig. 5A–C), indicating that NaB downregulates the expression of E2F1. The molecular docking results obtained using the standard precision method showed the interaction between BA and E2F1 (Supplementary Table 5). The protein E2F1–BA complex was visualized using PyMOL 2.1 for analysis (Fig. 5D–F). The molecular docking results indicated that BA binds well to the target protein E2F1, with a binding energy score of −6.07 kcal/mol. Visualization of the compound and protein complex using PyMOL 2.1 revealed the binding mode of the compound with the protein. The amino acid residues involved in the interaction between BA and the active sites of E2F1 included GLY-836, GLU-837, PRO-260, PHE-261, ILE-835, DER-838, THR-841, ILE-297, and ILE-262. The hydrophobic chain at one end of the BA compound interacts with the active-site amino acid PRO-260. The carboxyl group of the compound forms strong hydrogen bonds with GLY-836 and GLU-837, effectively anchoring the small molecules in the protein pocket. The compound also
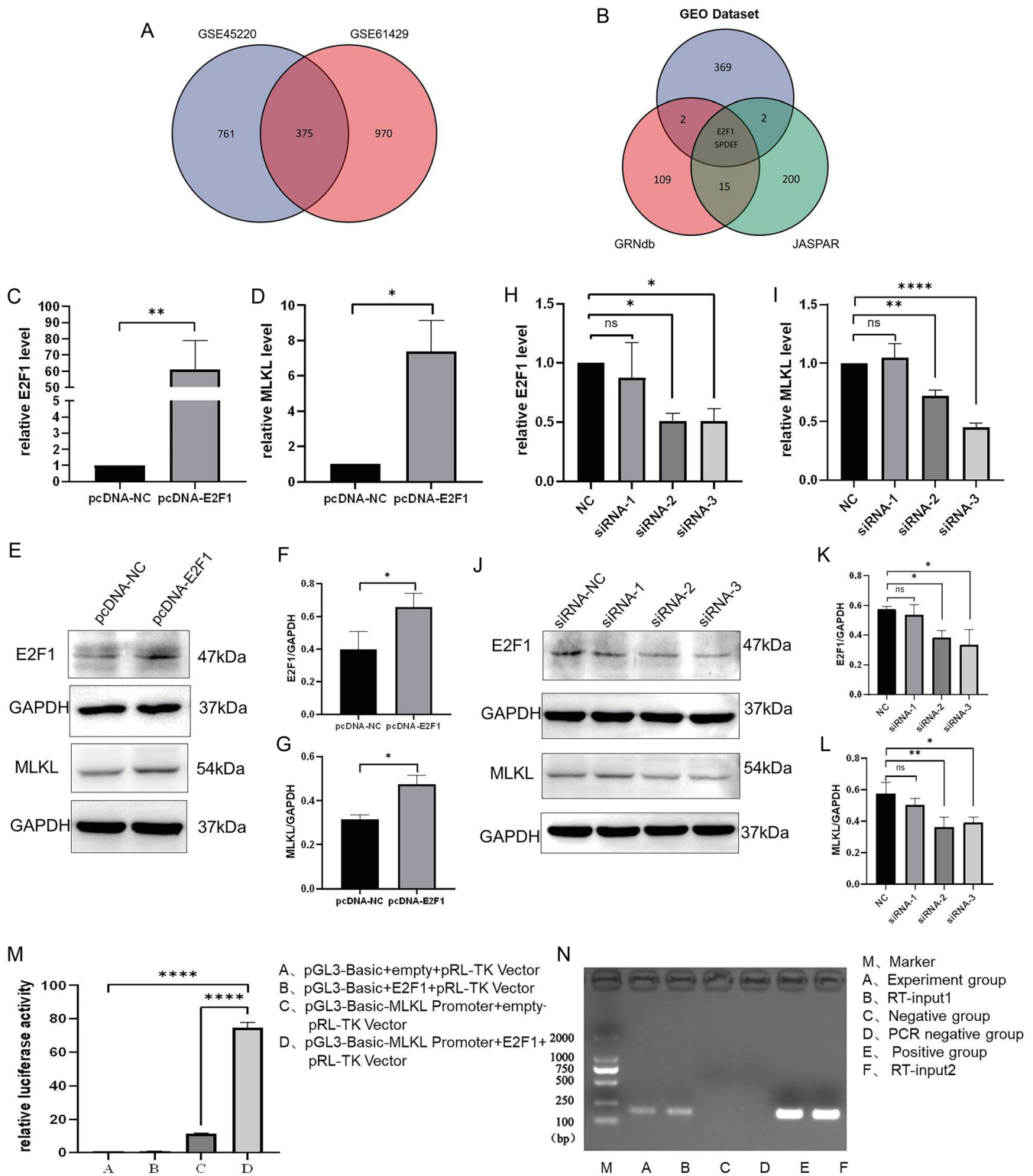
Fig. 4. The analysis of regulation for MLKL. (A, B) Differential gene analysis of GSE45220 (HT-29 cells were stimulated with NaB and unstimulated control, n = 3 in each group for 24 h) and GSE61429 datasets (butyrate-treated vs. untreated HT-29 cells; n = 2 in each group for 24 h) in the GEO database (Adj. *p*-value < 0.05 and |log2FC| > 1). Intersection of the predicted transcription factors from the JASPAR and GRNdb databases with the differentially expressed genes. (C–L) Overexpression of E2F1 plasmid and siRNA-E2F1 transfection were performed. qRT-PCR and Western blot were used to detect the mRNA and protein expression levels of MLKL. (M, N). Dual-luciferase reporter assay and ChIP experiment were used to detect the binding of E2F1 with the promoter region of MLKL. NaB, sodium butyrate; GEO, Gene Expression Omnibus; ChIP, chromatin immunoprecipitation; *p* < 0.05, **p* < 0.01, ****p* < 0.0001, ns, no significance.
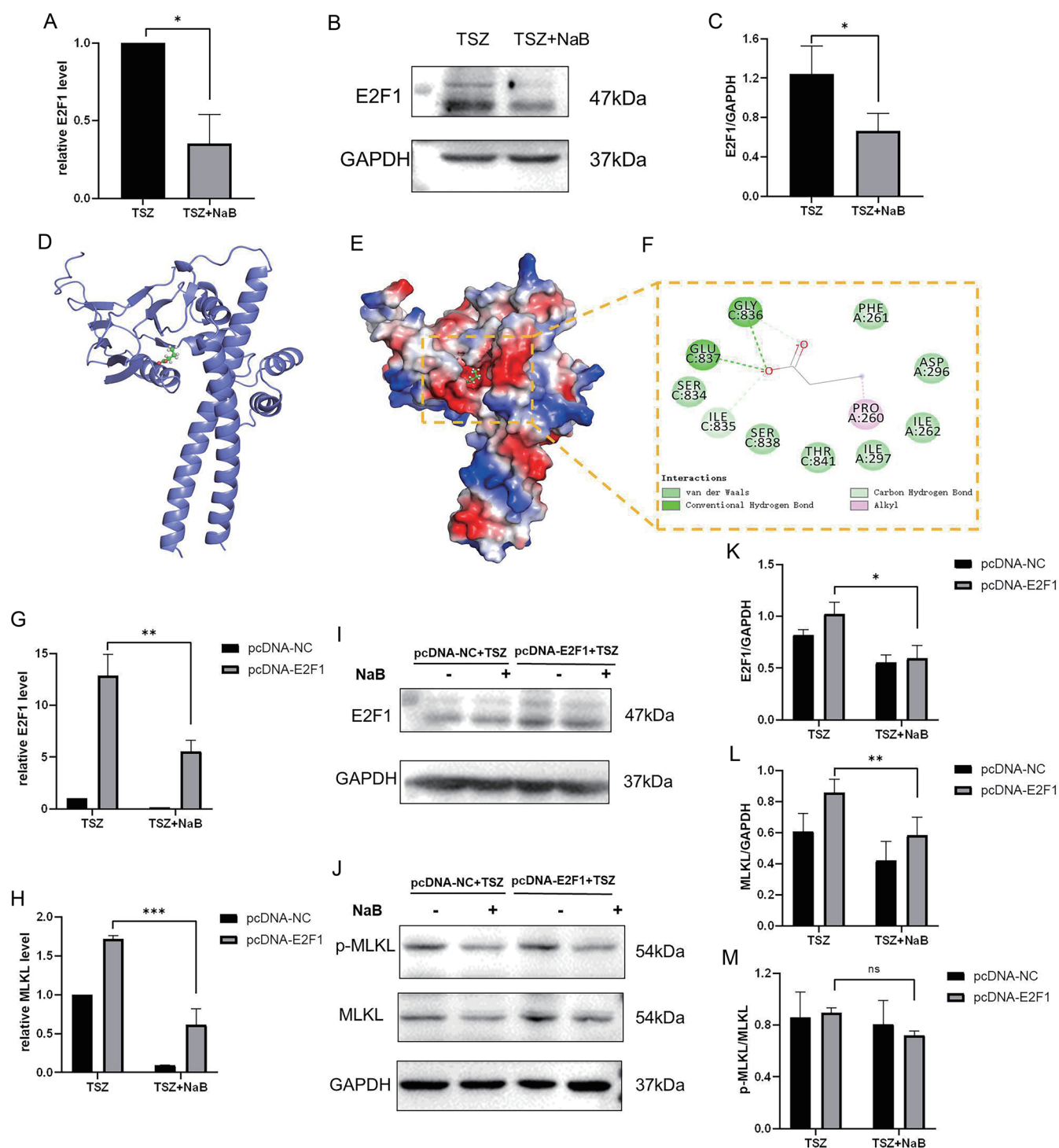
Fig. 5. The regulatory mechanism of NaB on necroptosis. (A–C) qRT-PCR and Western blot analysis of the effects of NaB on the mRNA and protein expression levels of E2F1. (D–F) Binding mode of E2F1 with BA. D) The 3D structure of the complex, E) Electrostatic surface of the protein, F) Detailed binding mode of the complex. (G–M) After transfection with the E2F1-overexpression plasmid, TSZ and NaB were added based on different groups. qRT-PCR and Western blot were performed for detection. NaB, sodium butyrate; BA, bile acid; +, addition of 4mM NaB; -, without NaB; *$p < 0.05$, **$p < 0.01$, ***$p < 0.001$, ns, no significance.

exhibits strong van der Waals interactions with surrounding residues. In summary, BA interacts well with the E2F1 target protein and can form stable complexes that strongly correlate with the protein target.

E2F1-overexpression plasmids and empty plasmids were first separately transfected into HT29 cell lines and then induced with the necroptosis inducer and NaB. qRT-PCR and Western blot analyses showed that in the E2F1-overexpres-

sion group, the addition of NaB decreased both the mRNA and protein expressions of E2F1 and MLKL ($p < 0.05$ for both), with no statistical difference in the p-MLKL protein expression ($p > 0.05$) (Fig. 5G–M). Therefore, it can be suggested that NaB alleviates necroptosis by downregulating MLKL via E2F1.

Discussion

Various studies have reported that necroptosis occurs during inflammation, regeneration, and fibrosis of the liver in diseases such as cirrhosis.[45] Han *et al*.[46] found significantly elevated mRNA levels of RIPK3 in patients with subacute liver failure caused by the hepatitis B virus, with RIPK3 and MLKL positively correlated with liver injury and poor prognosis. Zhang *et al*.[47] demonstrated a strong correlation between necroptosis and poor prognosis in patients with end-stage alcoholic liver cirrhosis. Afonso *et al*.[48] found elevated levels of RIPK3 in patients with non-alcoholic fatty liver, which correlated with liver inflammation and fibrosis. Another study by the authors confirmed the relationship between chronic inflammation, liver fibrosis, and necroptosis in aging livers.[49] Additionally, Zhang *et al*.[50] reported that patients with autoimmune hepatitis exhibited increased intestinal permeability and significant activation of RIPK3 in liver macrophages. We measured the levels of necroptosis markers in the serum of patients with liver cirrhosis and healthy individuals and found that RIPK3 and MLKL levels in patients with liver cirrhosis were higher than those in healthy individuals. These findings indicate the presence of necroptosis in patients with liver cirrhosis.

Zonulin is a 47-kDa prehaptoglobin-2 precursor synthesized by intestinal and liver cells and is widely used as a biological marker for intestinal permeability.[51] We noted a significant increase in the serum levels of Zonulin in patients with liver cirrhosis compared to healthy individuals, suggesting intestinal mucosal injury in these patients. Furthermore, correlation analysis showed a positive relationship between Zonulin, RIPK3, and MLKL, indicating a connection between intestinal mucosal injury and necroptosis in patients with liver cirrhosis. However, it remains unclear whether necroptosis occurs in IECs. Therefore, we conducted further animal experiments.

We successfully established a rat model of liver cirrhosis and observed intestinal mucosal injury in the model through HE staining. We measured the expression levels of tight junction proteins in the intestinal mucosa of rats from each group to ascertain the extent of damage to the intestinal mucosal barrier and to evaluate whether this damage correlated with necroptosis. The results indicated that the expressions of Claudin-1 and Occludin proteins were significantly reduced in the liver cirrhosis group, confirming damage to the intestinal mucosal barrier in rats with liver cirrhosis. However, we did not find any statistically significant difference in the expression of the ZO-1 protein, which differs from the findings of previous studies.[52] We next analyzed the expressions of MLKL and p-MLKL proteins in the IECs of the two groups of rats. Compared to the control group, the levels of MLKL and p-MLKL in the IECs of rats with liver cirrhosis were elevated, indicating necroptosis in the IECs of these rats.

Butyrate is an SCFA derived from the microbial fermentation of dietary fiber in the colon. It is rapidly absorbed by the colonic mucosa and is primarily used as an energy source by colonic cells, with only a small amount entering the bloodstream. Butyrate has been shown to possess anti-inflammatory properties and enhance the functional integrity of the intestinal barrier.[53] Studies have shown that bacteria producing butyrate salts, such as *Eubacterium rectale*,

Coprococcus eutacus, and *Anaerotruncus colihominis*, are significantly downregulated in patients with liver cirrhosis compared to healthy individuals.[54] Bloom *et al*.[55] recently reported that SCFAs are associated with the severity of liver cirrhosis and are closely related to hepatic encephalopathy and blood ammonia levels. Our study found that butyrate levels in the feces of patients with liver cirrhosis are lower than those in healthy individuals. We further conducted a correlation analysis between fecal butyrate levels and RIPK3 and MLKL, key molecules involved in necroptosis. The results indicated that butyrate is related to necroptosis and plays a negative regulatory role.

Previous studies have demonstrated the protective effects of NaB, with concentrations varying between 150 and 300 mmol/L, on the colonic epithelium in rat models.[56–59] We administered 200 mmol/L·d·kg of NaB to our experimental group and measured the butyrate content in their feces. We found that butyrate levels in the feces of rats in the liver cirrhosis group were lower than those in the negative control group, consistent with the results observed in patients with liver cirrhosis and healthy controls. Additionally, we found that NaB can reduce the expression of MLKL in the IECs of rats with liver cirrhosis. Thus, NaB may alleviate necroptosis of IECs in patients with cirrhosis and protect the intestinal mucosal barrier. However, recent research by Wang K *et al*.[60] contradicts our findings, showing that butyrate induces developmental stage-dependent intestinal injury resembling necrotizing enterocolitis. In their study, FVB/N mice aged 14 or 28 days were used for *in vivo* injury studies, with 150 mM NaB injected directly into the intestinal lumen after exposing the ileocecal junction. Previous studies have indicated that low concentrations of butyrate have a protective effect on the intestinal mucosa, while high concentrations have the opposite effect.[61] The intestinal mucosa of neonatal mice is more fragile than that of adult mice, so the age of the mice, butyrate concentration, and method of administration may account for these differing results. Furthermore, we observed that the expression of Claudin-1 increased in the NaB group, although there were no statistically significant differences in the expression levels of ZO-1 and Occludin. Wang *et al*.[62] confirmed that NaB decreases intestinal permeability, increases the expression of the tight junction protein Claudin-1, and induces the redistribution of ZO-1 and Occludin on the cell membrane. The expression levels of tight junction proteins in each group were consistent with the status of necroptosis markers.

Necroptosis is typically initiated by the interaction of death signaling molecules (TNFα and FAS) with their respective membrane receptors. Activated RIPK1 interacts with RIPK3, leading to the autophosphorylation of RIPK3 and the formation of the RIPK1–RIPK3–MLKL complex. The activation loop of the pseudokinase domain of MLKL is phosphorylated by RIPK3, causing MLKL to translocate to the cell membrane. Consequently, cell membrane permeability increases, leading to cell death. Phosphorylated MLKL is a marker of the execution of necroptosis.[63] MLKL can act as a client protein and interact with various molecular chaperone proteins. Heat shock protein 90, through its co-chaperone CDC37, binds to the pseudokinase domain of MLKL and may be involved in the phosphorylation of MLKL. Heat shock protein 70 stabilizes and promotes MLKL oligomerization by binding to its N-terminal region.[64] Conversely, Beclin1 and Bcl-2 can bind to the coiled-coil domain and the Bcl-2 homology domain of MLKL, respectively, inhibiting necroptosis.[65,66] In the present study, our results revealed that NaB had no regulatory effect on RIPK1 and RIPK3, while the mRNA and protein expressions of MLKL were significantly decreased, with no apparent change in the

p-MLKL/MLKL ratio. Therefore, we suggest that NaB regulates the expression of MLKL at the transcriptional level.

Next, we predicted that the transcription factor E2F1 could bind to MLKL. E2F1 is involved in the regulation of the cell cycle and apoptosis.[67] The HT29 cell line was transfected with E2F1-overexpression plasmids and subjected to RNA interference for E2F1 to achieve overexpression and knockdown, respectively. As a result, the mRNA and protein expressions of MLKL were correspondingly upregulated and downregulated, suggesting that E2F1 regulates the expression of MLKL. Through dual-luciferase reporter assays and the ChIP experiment, we confirmed that E2F1 can bind to the promoter region of MLKL.

We utilized the GEO database to analyze genes in IECs regulated by NaB and observed a downregulation in the expression of E2F1. We reached the same conclusion through *in vitro* cell experiments. The results of molecular docking showed that BA binds well to the target protein, with a binding energy score of −6.07 kcal/mol. Thus, it can be suggested that NaB can bind to E2F1. After transfecting with E2F1-overexpression plasmids to induce necroptosis, the expression level of MLKL increased. The addition of NaB reduced the MLKL level, while the p-MLKL/MLKL ratio remained unchanged, indicating that NaB reduces the transcriptional expression of MLKL by decreasing E2F1, without affecting the subsequent phosphorylation of MLKL.

Conclusions

This study demonstrated that intestinal mucosal injury in cirrhosis is closely associated with the necroptosis of IECs. NaB alleviates intestinal mucosal injury in cirrhosis and protects the intestinal barrier by reducing necroptosis in IECs. E2F1, a transcription factor, regulates MLKL, and BA has a strong binding affinity for E2F1. NaB inhibits necroptosis in IECs by reducing the expression of E2F1, thereby downregulating the expression level of MLKL. This regulatory process contributes to the protection of the intestinal barrier. These findings provide a new direction for future clinical treatments of cirrhosis and its complications, as well as for the development of new therapeutic drugs.

Funding

Conflict of interest

XD has been an Associate Editor of *Journal of Clinical and Translational Hepatology* since 2013. The other authors have no conflicts of interest related to this publication.

Author contributions

Study conception and design (CZ, XD, YZ), performance of experiments (YZ, ZW, YL, BL), analysis of the data (YZ, CZ, XD, YD, YL, QS, CH, YF), funding acquisition (YD), drafting of the manuscript (YZ), and revision of the manuscript (CZ, XD). All authors have made significant contributions to this work and have approved the final manuscript.

Ethical statement

All procedures involving human participants complied with the Declaration of Helsinki. The study was approved by the Ethics Committee of Shengjing Hospital of China Medical University (No. 2020PS316K). All animal experiments were also approved by the Ethics Committee of Shengjing Hospital of China Medical University (No. 2023PS262K). All patients provided written informed consent. All animals received human care.

Data sharing statement

The data used to support the findings of this study are available from the corresponding author upon request.

References

[1] Ginès P, Castera L, Lammert F, Graupera I, Serra-Burriel M, Allen AM, *et al*. Population screening for liver fibrosis: Toward early diagnosis and intervention for chronic liver diseases. Hepatology 2022;75(1):219–228. doi:10.1002/hep.32163, PMID:34537988.

[2] Tapper EB, Parikh ND. Diagnosis and Management of Cirrhosis and Its Complications: A Review. JAMA 2023;329(18):1589–1602. doi:10.1001/jama.2023.5997, PMID:37159031.

[3] Mohandas S, Vairappan B. Pregnane X receptor activation by its natural ligand Ginkgolide-A improves tight junction proteins expression and attenuates bacterial translocation in cirrhosis. Chem Biol Interact 2020;315:108891. doi:10.1016/j.cbi.2019.108891, PMID:31697926.

[4] Del Bo' C, Bernardi S, Cherubini A, Porrini M, Gargari G, Hidalgo-Liberona N, *et al*. A polyphenol-rich dietary pattern improves intestinal permeability, evaluated as serum zonulin levels, in older subjects: The MaPLE randomised controlled trial. Clin Nutr 2021;40(5):3006–3018. doi:10.1016/j.clnu.2020.12.014, PMID:33388204.

[5] Tao S, Xiong Y, Han D, Pi Y, Zhang H, Wang J. N-(3-oxododecanoyl)-l-homoserine lactone disrupts intestinal epithelial barrier through triggering apoptosis and collapsing extracellular matrix and tight junction. J Cell Physiol 2021;236(8):5771–5784. doi:10.1002/jcp.30261, PMID:33400297.

[6] Otsubo K, Maeyashiki C, Nibe Y, Tamura A, Aonuma E, Matsuda H, *et al*. Receptor-Interacting Protein Kinase 3 (RIPK3) inhibits autophagic flux during necroptosis in intestinal epithelial cells. FEBS Lett 2020;594(10):1586–1595. doi:10.1002/1873-3468.13748, PMID:31997355.

[7] Zhong Q, Roumeliotis TI, Kozik Z, Cepeda-Molero M, Fernández LÁ, Shenoy AR, *et al*. Clustering of Tir during enteropathogenic E. coli infection triggers calcium influx-dependent pyroptosis in intestinal epithelial cells. PLoS Biol 2020;18(12):e3000986. doi:10.1371/journal.pbio.3000986, PMID:33378358.

[8] Shi Y, Cui X, Sun Y, Zhao Q, Liu T. Intestinal vitamin D receptor signaling ameliorates dextran sulfate sodium-induced colitis by suppressing necroptosis of intestinal epithelial cells. FASEB J 2020;34(10):13494–13506. doi:10.1096/fj.202000143RRR, PMID:32779265.

[9] Mayr L, Grabherr F, Schwärzler J, Reitmeier I, Sommer F, Gehmacher T, *et al*. Dietary lipids fuel GPX4-restricted enteritis resembling Crohn's disease. Nat Commun 2020;11(1):1775. doi:10.1038/s41467-020-15646-6, PMID:32286299.

[10] Jiang X, Deng W, Tao S, Tang Z, Chen Y, Tian M, *et al*. A RIPK3-independent role of MLKL in suppressing parthanatos promotes immune evasion in hepatocellular carcinoma. Cell Discov 2023;9(1):7. doi:10.1038/s41421-022-00504-0, PMID:36650126.

[11] Negroni A, Colantoni E, Pierdomenico M, Palone F, Costanzo M, Oliva S, *et al*. RIP3 AND pMLKL promote necroptosis-induced inflammation and alter membrane permeability in intestinal epithelial cells. Dig Liver Dis 2017;49(11):1201–1210. doi:10.1016/j.dld.2017.08.017, PMID:28844856.

[12] Zhang X, Wu J, Liu Q, Li X, Li S, Chen J, *et al*. mtDNA-STING pathway promotes necroptosis-dependent enterocyte injury in intestinal ischemia reperfusion. Cell Death Dis 2020;11(12):1050. doi:10.1038/s41419-020-03239-6, PMID:33311495.

[13] Liu Y, Xu Q, Wang Y, Liang T, Li X, Wang D, *et al*. Necroptosis is active and contributes to intestinal injury in a piglet model with lipopolysaccharide challenge. Cell Death Dis 2021;12(1):62. doi:10.1038/s41419-020-03365-1, PMID:33431831.

[14] Zhao Q, Guo J, Cheng X, Liao Y, Bi Y, Gong Y, *et al*. RIPK3 Suppresses the Progression of Spontaneous Intestinal Tumorigenesis. Front Oncol 2021;11:664927. doi:10.3389/fonc.2021.664927, PMID:33996591.

[15] Liu T, Zong H, Chen X, Li S, Liu Z, Cui X, *et al*. Toll-like receptor 4-mediated necroptosis in the development of necrotizing enterocolitis. Pediatr Res 2022;91(1):73–82. doi:10.1038/s41390-021-01457-y, PMID:33731807.

[16] Efremova I, Maslennikov R, Medvedev O, Kudryavtseva A, Avdeeva A, Krasnov G, *et al*. Gut Microbiota and Biomarkers of Intestinal Barrier Damage in Cirrhosis. Microorganisms 2024;12(3):463. doi:10.3390/microorganisms12030463, PMID:38543514.

[17] Pabst O, Hornef MW, Schaap FG, Cerovic V, Clavel T, Bruns T. Gut-liver axis: barriers and functional circuits. Nat Rev Gastroenterol Hepatol 2023;20(7):447–461. doi:10.1038/s41575-023-00771-6, PMID:37085614.

[18] Trebicka J, Macnaughtan J, Schnabl B, Shawcross DL, Bajaj JS. The microbiota in cirrhosis and its role in hepatic decompensation. J Hepatol 2021;75(Suppl 1):S67–S81. doi:10.1016/j.jhep.2020.11.013, PMID:34039493.

[19] Wang R, Cao S, Bashir MEH, Hesser LA, Su Y, Hong SMC, *et al*. Treatment

of peanut allergy and colitis in mice via the intestinal release of butyrate from polymeric micelles. Nat Biomed Eng 2023;7(1):38–55. doi:10.1038/s41551-022-00972-5, PMID:36550307.

[20] Zhou Z, Xu N, Matei N, McBride DW, Ding Y, Liang H, *et al*. Sodium butyrate attenuated neuronal apoptosis via GPR41/Gβγ/PI3K/Akt pathway after MCAO in rats. J Cereb Blood Flow Metab 2021;41(2):267–281. doi:10.1177/0271678X20910533, PMID:32151222.

[21] Roshanravan N, Alamdari NM, Jafarabadi MA, Mohammadi A, Shabestari BR, Nasirzadeh N, *et al*. Effects of oral butyrate and inulin supplementation on inflammation-induced pyroptosis pathway in type 2 diabetes: A randomized, double-blind, placebo-controlled trial. Cytokine 2020;131:155101. doi:10.1016/j.cyto.2020.155101, PMID:32315958.

[22] Zhao Y, Li J, Guo W, Li H, Lei L. Periodontitis-level butyrate-induced ferroptosis in periodontal ligament fibroblasts by activation of ferritinophagy. Cell Death Discov 2020;6(1):119. doi:10.1038/s41420-020-00356-1, PMID:33298848.

[23] Palomino-Kobayashi LA, Ymaña B, Ruiz J, Mayanga-Herrera A, Ugarte-Gil MF, Pons MJ. Zonulin, a marker of gut permeability, is associated with mortality in a cohort of hospitalised peruvian COVID-19 patients. Front Cell Infect Microbiol 2022;12:1000291. doi:10.3389/fcimb.2022.1000291, PMID:36147602.

[24] Gao T, Zhang H, Li Q, Zhao F, Wang N, He W, *et al*. Fuzi decoction treats chronic heart failure by regulating the gut microbiota, increasing the short-chain fatty acid levels and improving metabolic disorders. J Pharm Biomed Anal 2023;236:115693. doi:10.1016/j.jpba.2023.115693, PMID:37696191.

[25] Regimbeau JM, Fuks D, Kohneh-Shahri N, Terris B, Soubrane O. Restrictive model of compensated carbon tetrachloride-induced cirrhosis in rats. World J Gastroenterol 2008;14(45):6943–6947. doi:10.3748/wjg.14.6943, PMID:19058329.

[26] Qin JJ, Mao W, Wang X, Sun P, Cheng D, Tian S, *et al*. Caspase recruitment domain 6 protects against hepatic ischemia/reperfusion injury by suppressing ASK1. J Hepatol 2018;69(5):1110–1122. doi:10.1016/j.jhep.2018.06.014, PMID:29958938.

[27] Chiu CJ, McArdle AH, Brown R, Scott HJ, Gurd FN. Intestinal mucosal lesion in low-flow states. I. A morphological, hemodynamic, and metabolic reappraisal. Arch Surg 1970;101(4):478–483. doi:10.1001/archsurg.1970.01340280030009, PMID:5457245.

[28] Sun L, Yang S, Deng Q, Dong K, Li Y, Wu S, *et al*. Salmonella Effector SpvB Disrupts Intestinal Epithelial Barrier Integrity for Bacterial Translocation. Front Cell Infect Microbiol 2020;10:606541. doi:10.3389/fcimb.2020.606541, PMID:33392110.

[29] Kong X, Ai G, Wang D, Chen R, Guo D, Yao Y, *et al*. PDE4 and Epac1 Synergistically Promote Rectal Carcinoma via the cAMP Pathway. Anal Cell Pathol (Amst) 2019;2019:7145198. doi:10.1155/2019/7145198, PMID:30809467.

[30] Zhang SQ, Deng Q, Zhu Q, Hu ZL, Long LH, Wu PF, *et al*. Cell type-specific NRBF2 orchestrates autophagic flux and adult hippocampal neurogenesis in chronic stress-induced depression. Cell Discov 2023;9(1):90. doi:10.1038/s41421-023-00583-7, PMID:37644025.

[31] Park HH, Kim HR, Park SY, Hwang SM, Hong SM, Park S, *et al*. RIPK3 activation induces TRIM28 derepression in cancer cells and enhances the anti-tumor microenvironment. Mol Cancer 2021;20(1):107. doi:10.1186/s12943-021-01399-3, PMID:34419074.

[32] Barrett T, Wilhite SE, Ledoux P, Evangelista C, Kim IF, Tomashevsky M, *et al*. NCBI GEO: archive for functional genomics data sets—update. Nucleic Acids Res 2013;41(Database issue):D991–D995. doi:10.1093/nar/gks1193, PMID:23193258.

[33] Dasgupta N, Kumar Thakur B, Chakraborty A, Das S. Butyrate-Induced In Vitro Colonocyte Differentiation Network Model Identifies ITGB1, SYK, CDKN2A, CHAF1A, and LRP1 as the Prognostic Markers for Colorectal Cancer Recurrence. Nutr Cancer 2019;71(2):257–271. doi:10.1080/01635581.2018.1540715, PMID:30475060.

[34] Ritchie ME, Phipson B, Wu D, Hu Y, Law CW, Shi W, *et al*. limma powers differential expression analyses for RNA-sequencing and microarray studies. Nucleic Acids Res 2015;43(7):e47. doi:10.1093/nar/gkv007, PMID:25605792.

[35] Bryne JC, Valen E, Tang MH, Marstrand T, Winther O, da Piedade I, *et al*. JASPAR, the open access database of transcription factor-binding profiles: new content and tools in the 2008 update. Nucleic Acids Res 2008;36(Database issue):D102–D106. doi:10.1093/nar/gkm955, PMID:18006571.

[36] Fang L, Li Y, Ma L, Xu Q, Tan F, Chen G. GRNdb: decoding the gene regulatory networks in diverse human and mouse conditions. Nucleic Acids Res 2021;49(D1):D97–D103. doi:10.1093/nar/gkaa995, PMID:33151298.

[37] Gharaati-Far N, Tohidkia MR, Dehnad A, Omidi Y. Efficiency and cytotoxicity analysis of cationic lipids-mediated gene transfection into AGS gastric cancer cells. Artif Cells Nanomed Biotechnol 2018;46(5):1001–1008. doi:10.1080/21691401.2017.1355311, PMID:28728449.

[38] Li Y, Ouyang Q, Chen Z, Chen W, Zhang B, Zhang S, *et al*. Intracellular labile iron is a key regulator of hepcidin expression and iron metabolism. Hepatol Int 2023;17(3):636–647. doi:10.1007/s12072-022-10452-2, PMID:36512269.

[39] Li L, Li L, Shao Y, Du R, Li L, Shi X, *et al*. Calcium/calmodulin dependent protein kinase IV in trophoblast cells under insulin resistance: functional and metabolomic analyses. Mol Med 2023;29(1):82. doi:10.1186/s10020-023-00669-8, PMID:37386367.

[40] Zheng Y, Wang N, Wang S, Zhang J, Yang B, Wang Z. Chronic psychological stress promotes breast cancer pre-metastatic niche formation by mobilizing splenic MDSCs via TAM/CXCL1 signaling. J Exp Clin Cancer Res 2023;42(1):129. doi:10.1186/s13046-023-02696-z, PMID:37210553.

[41] Fazi R, Tintori C, Brai A, Botta L, Selvaraj M, Garbelli A, *et al*. Homology Model-Based Virtual Screening for the Identification of Human Helicase DDX3 Inhibitors. J Chem Inf Model 2015;55(11):2443–2454. doi:10.1021/acs.jcim.5b00419, PMID:26544088.

[42] Rajeswari M, Santhi N, Bhuvaneswari V. Pharmacophore and Virtual Screening of JAK3 inhibitors. Bioinformation 2014;10(3):157–163. doi:10.6026/97320630010157, PMID:24748756.

[43] Morris GM, Huey R, Lindstrom W, Sanner MF, Belew RK, Goodsell DS, *et al*. AutoDock4 and AutoDockTools4: Automated docking with selective receptor flexibility. J Comput Chem 2009;30(16):2785–2791. doi:10.1002/jcc.21256, PMID:19399780.

[44] Shlomovitz I, Zargarian S, Erlich Z, Edry-Botzer L, Gerlic M. Distinguishing Necroptosis from Apoptosis. Methods Mol Biol 2018;1857:35–51. doi:10.1007/978-1-4939-8754-2_4, PMID:30136228.

[45] Li X, Dong G, Xiong H, Diao H. A narrative review of the role of necroptosis in liver disease: a double-edged sword. Ann Transl Med 2021;9(5):422. doi:10.21037/atm-20-5162, PMID:33842643.

[46] Han L, Teng Y, Fan Y, Gao S, Li F, Wang K. Receptor-Interacting Protein Kinase 3 (RIPK3) mRNA Levels Are Elevated in Blood Mononuclear Cells of Patients with Poor Prognosis of Acute-on-Chronic Hepatitis B Liver Failure. Tohoku J Exp Med 2019;247(4):237–245. doi:10.1620/tjem.247.237, PMID:30996211.

[47] Zhang Z, Xie G, Liang L, Liu H, Pan J, Cheng H, *et al*. RIPK3-Mediated Necroptosis and Neutrophil Infiltration Are Associated with Poor Prognosis in Patients with Alcoholic Cirrhosis. J Immunol Res 2018;2018:1509851. doi:10.1155/2018/1509851, PMID:30596105.

[48] Afonso MB, Rodrigues PM, Mateus-Pinheiro M, Simão AL, Gaspar MM, Majdi A, *et al*. RIPK3 acts as a lipid metabolism regulator contributing to inflammation and carcinogenesis in non-alcoholic fatty liver disease. Gut 2021;70(12):2359–2372. doi:10.1136/gutjnl-2020-321767, PMID:33361348.

[49] Mohammed S, Thadathil N, Selvarani R, Nicklas EH, Wang D, Miller BF, *et al*. Necroptosis contributes to chronic inflammation and fibrosis in aging liver. Aging Cell 2021;20(12):e13512. doi:10.1111/acel.13512, PMID:34761505.

[50] Zhang H, Liu M, Zhong W, Zheng Y, Li Y, Guo L, *et al*. Leaky Gut Driven by Dysbiosis Augments Activation and Accumulation of Liver Macrophages via RIP3 Signaling Pathway in Autoimmune Hepatitis. Front Immunol 2021;12:624360. doi:10.3389/fimmu.2021.624360, PMID:33841405.

[51] Voulgaris TA, Karagiannakis D, Hadziyannis E, Manolakopoulos S, Karamanolis GP, Papatheodoridis G, *et al*. Serum zonulin levels in patients with liver cirrhosis: Prognostic implications. World J Hepatol 2021;13(10):1394–1404. doi:10.4254/wjh.v13.i10.1394, PMID:34786174.

[52] Wang PF, Yao DH, Hu YY, Li Y. Vitamin D Improves Intestinal Barrier Function in Cirrhosis Rats by Upregulating Heme Oxygenase-1 Expression. Biomol Ther (Seoul) 2019;27(2):222–230. doi:10.4062/biomolther.2018.052, PMID:30173501.

[53] Tabat MW, Marques TM, Markgren M, Löfvendahl L, Brummer RJ, Wall R. Acute Effects of Butyrate on Induced Hyperpermeability and Tight Junction Protein Expression in Human Colonic Tissues. Biomolecules 2020;10(5):766. doi:10.3390/biom10050766, PMID:32422994.

[54] Shao L, Ling Z, Chen D, Liu Y, Yang F, Li L. Disorganized Gut Microbiome Contributed to Liver Cirrhosis Progression: A Meta-Omics-Based Study. Front Microbiol 2018;9:3166. doi:10.3389/fmicb.2018.03166, PMID:30631318.

[55] Bloom PP, Luévano JM Jr, Miller KJ, Chung RT. Deep stool microbiome analysis in cirrhosis reveals an association between short-chain fatty acids and hepatic encephalopathy. Ann Hepatol 2021;25:100333. doi:10.1016/j.aohep.2021.100333, PMID:33621653.

[56] Dou X, Ma Z, Yan D, Gao N, Li Z, Li Y, *et al*. Sodium butyrate alleviates intestinal injury and microbial flora disturbance induced by lipopolysaccharides in rats. Food Funct 2022;13(3):1360–1369. doi:10.1039/d1fo03183j, PMID:35044411.

[57] Peña-Rodríguez M, Vega-Magaña N, García-Benavides L, Zepeda-Nuño JS, Gutierrez-Silerio GY, González-Hernández LA, *et al*. Butyrate administration strengthens the intestinal epithelium and improves intestinal dysbiosis in a cholestasis fibrosis model. J Appl Microbiol 2022;132(1):571–583. doi:10.1111/jam.15135, PMID:33982373.

[58] Xiao S, Jing S, Jiakui S, Lei Z, Ying L, Han L, *et al*. Butyrate Ameliorates Intestinal Epithelial Barrier Injury Via Enhancing Foxp3+ Regulatory T-Cell Function in Severe Acute Pancreatitis Model. Turk J Gastroenterol 2022;33(8):710–719. doi:10.5152/tjg.2022.21307, PMID:35943149.

[59] Zhou B, Te Ba, Wang L, Gao Y, He Q, Yan Z, *et al*. Combination of sodium butyrate and probiotics ameliorates severe burn-induced intestinal injury by inhibiting oxidative stress and inflammatory response. Burns 2022;48(5):1213–1220. doi:10.1016/j.burns.2021.11.009, PMID:34903409.

[60] Wang K, Tao GZ, Salimi-Jazi F, Lin PY, Sun Z, Liu B, *et al*. Butyrate induces development-dependent necrotizing enterocolitis-like intestinal epithelial injury via necroptosis. Pediatr Res 2023;93(4):801–809. doi:10.1038/s41390-022-02333-z, PMID:36202969.

[61] Nielsen DSG, Jensen BB, Theil PK, Nielsen TS, Knudsen KEB, Purup S. Effect of butyrate and fermentation products on epithelial integrity in a mucus-secreting human colon cell line. J Funct Foods 2018;40:9–17. doi:10.1016/j.jff.2017.10.023.

[62] Wang HB, Wang PY, Wang X, Wan YL, Liu YC. Butyrate enhances intestinal epithelial barrier function via up-regulation of tight junction protein Claudin-1 transcription. Dig Dis Sci 2012;57(12):3126–3135. doi:10.1007/s10620-012-2259-4, PMID:22684624.

[63] Garnish SE, Martin KR, Kauppi M, Jackson VE, Ambrose R, Eng VV, *et al*. A common human MLKL polymorphism confers resistance to negative regu-

lation by phosphorylation. Nat Commun 2023;14(1):6046. doi:10.1038/s41467-023-41724-6, PMID:37770424.

[64] Johnston AN, Ma Y, Liu H, Liu S, Hanna-Addams S, Chen S, *et al*. Necroptosis-blocking compound NBC1 targets heat shock protein 70 to inhibit MLKL polymerization and necroptosis. Proc Natl Acad Sci U S A 2020;117(12):6521–6530. doi:10.1073/pnas.1916503117, PMID:32156734.

[65] Kamal AM, Nabih NA, Rakha NM, Sanad EF. Upregulation of necroptosis markers RIPK3/MLKL and their crosstalk with autophagy-related protein Beclin-1 in primary immune thrombocytopenia. Clin Exp Med 2023;23(2):447–456. doi:10.1007/s10238-022-00839-8, PMID:35699825.

[66] Baik JY, Liu Z, Jiao D, Kwon HJ, Yan J, Kadigamuwa C, *et al*. ZBP1 not RIPK1 mediates tumor necroptosis in breast cancer. Nat Commun 2021;12(1):2666. doi:10.1038/s41467-021-23004-3, PMID:33976222.

[67] Kassab A, Gupta I, Moustafa AA. Role of E2F transcription factor in oral cancer: Recent insight and advancements. Semin Cancer Biol 2023;92:28–41. doi:10.1016/j.semcancer.2023.03.004, PMID:36924812.